Catalysis Science & Technology

PAPER

View Article Online
View Journal | View Issue

Cite this: *Catal. Sci. Technol.*, 2015, 5, 1813

Received 5th November 2014,
Accepted 18th December 2014

DOI: 10.1039/c4cy01445f

www.rsc.org/catalysis

Conversion of dimethyl ether to toluene under an O_2 stream over W/HZSM-5 catalysts

Bo Wang,†[ab] Hui Wang,*[a] Guangbo Liu,*[a] Xuemin Li[ab] and Jinhu Wu*[a]

The direct conversion of dimethyl ether (DME) to toluene without other aromatics is realized over W/HZSM-5 catalysts with high W contents. The influence of W content on the nature of tungsten species, the distribution of acid sites, the redox properties, and the subsequent catalytic performance of W/HZSM-5 in DME conversion was investigated. The introduction of a high content of W in HZSM-5 can bring about some new redox sites and acidic sites associated with W species, although they also cover some acidic sites in HZSM-5. In this way, the introduction of W interrupts the dual cycle of the DME-to-hydrocarbon reaction on HZSM-5, and effectively the formation of higher methylbenzenes is limited.

1. Introduction

Dimethyl ether (DME) can be synthesized in one step from syngas with an elevated maximum conversion, which makes it a promising candidate as clean and highly efficient energy.[1–3] DME can replace liquefied petroleum gas, and it is also an attractive eco-friendly fuel for vehicles due to its superior combustion properties.[4] Not only limited to energy products, accompanied by an enlarged DME industry, DME is also an essential starting material or intermediate for value-added chemicals. At present, some catalytic conversion reactions of DME have been explored and progress has been achieved. Generally, the DME molecule can be easily activated to form CH_3-, CH_3O- and CH_3OCH_2-groups. Then the active groups can form hydrocarbons, like olefins, gasoline and aromatics,[5–7] through the hydrocarbon pool (HP) mechanism, or they can form oxygenated compounds such as methyl acetate,[8] formaldehyde (FA),[9] dimethoxymethane (DMM),[10,11] methyl formate (MF),[12] and ethanol.[13]

Concerning the catalysts, DME catalytic conversion is usually conducted on solid acidic catalysts like zeolite. In particular, the zeolite ZSM-5, distinguished by shape selectivity and good acidic properties, exhibits a high activity in the conversion of DME to hydrocarbons in a fixed-bed reactor with a slow deactivation rate.[14–16] Moreover, transition metal oxides have usually been used to modify zeolite properties to enhance the catalytic activity and selectivity, because of the ability of accommodating the acidity of zeolite and the enhancement of the activation of the DME molecule under an O_2 atmosphere at lower temperatures, thus adjusting the product distribution.[17] Among these transition metals, tungsten oxide gives strong Brønsted acid sites, either as bulk or supported oxides, but their structure and catalytic properties are strongly influenced by the support.[18] Several studies have explored how interactions between the support and tungsten oxide domains affect catalytic performance. Indeed, even for a given WO_x support system, WO_x domains exhibit a range of surface structures that depend strongly on synthetic protocols, such as the WO_x precursor and content, as well as on the thermal history of these materials.[19–21] Yang *et al.* reported that the W/HZSM-5 catalyst was a good dehydroaromatization catalyst in the presence of oxygen.[22] Also, Liu *et al.* obtained trace toluene from DME oxidation to ethanol over HZSM-5 catalysts with low tungsten contents (<23 wt.%) without any other aromatic products.[23] Reasonably, it is possible to obtain toluene with high selectivity from DME conversion through tuning the synergic effect of tungsten and HZSM-5. However, there have been no reports on the direct conversion of DME to toluene over W/HZSM-5 catalysts.

In this work, a novel route for the synthesis of toluene from DME by direct conversion over W/HZSM-5 in the presence of oxygen was studied. Catalysts with relatively high W contents were prepared and characterized by X-ray diffraction (XRD), N_2 adsorption, ultraviolet visible spectroscopy (UV-vis), X-ray photoelectron spectroscopy (XPS), temperature-programmed desorption of ammonia (NH_3-TPD) and temperature-programmed reduction of hydrogen (H_2-TPR). The influence of the W content on the distribution of acid sites, the redox

[a] *Key Laboratory of Biofuels, Qingdao Institute of Bioenergy and Bioprocess Technology, Chinese Academy of Sciences, Qingdao, 266101, PR China. E-mail: huiwangsun@gmail.com, liugb@qibebt.ac.cn, wujh@qibebt.ac.cn; Fax: +86 532 80662761; Tel: +86 532 80662764*

[b] *University of Chinese Academy of Sciences, Beijing 100049, PR China*

† Present address: Shanghai Key Laboratory of Green Chemistry and Chemical Processes, East China Normal University, Shanghai, China.

properties, the nature of tungsten species, and the subsequent catalytic performance of W/HZSM-5 in DME conversion to toluene was investigated.

2. Experimental

2.1 Catalyst preparation

The W/HZSM-5 catalysts were prepared by a wet impregnation method, as described elsewhere.[24] To obtain catalysts with different tungsten contents, the HZSM-5 powder (supplied by Shandong Qilu Huaxin High-tech Company) was first infiltrated in a thermostatted water bath (80 °C) with aqueous solutions of ammonium metatungstate containing the desired amount of $(NH_4)_6W_{12}O_{40}{\cdot}xH_2O$. The resulting material was then dried at 110 °C for 10 h with subsequent calcination at 500 °C for 5 h. The concentration of W was adjusted with nominal values of W content (25, 35, 45, 50 and 55 wt.%). The catalyst obtained was then expressed as x W/HZSM-5. The actual W contents x were determined by inductively coupled plasma-atomic emission spectrometry (ICP-AES), as shown in Table 1.

2.2 Catalyst characterization

X-ray diffraction (XRD) analysis was carried out by using a Bruker D8 Advance X-ray diffractometer with monochromatic high-intensity Cu Kα radiation (λ = 1.5418 Å) in the 2θ range of 5–70° operated at 30 kV and 30 mA.

Nitrogen adsorption/desorption isotherms were measured at −196 °C on a Micromeritics ASAP 2020 adsorption apparatus. Before the measurements, the samples were degassed at 300 °C for more than 6 h under high vacuum conditions. The Brunauer–Emmett–Teller (BET) method was utilized to calculate the specific surface areas (S_{BET}). The pore size distribution was derived from the adsorption branch by the Barrett–Joyner–Halenda (BJH) method. The total pore volumes were estimated from the adsorbed amount at a relative pressure P/P_0 of 0.99.

Diffuse reflectance UV-vis spectra were performed on a Hitachi U-4100 spectrophotometer equipped with a diffuse reflectance attachment. Spectra were recorded at room temperature in the wavelength range 200–800 nm.

XPS was obtained on a Quantum-2000 Scanning ESCA Microprobe instrument using an Al Kα X-ray radiation source. The pressure in the analysis equipment was maintained below 10^{-6} Pa during the data acquisition. The passing energy of the experiment was 46.95 eV, and all the binding energy measured was calibrated with contaminated carbon (284.6 eV) as reference. The spectra were decomposed by using XPSPEAK software (Ver. 4.1) after applying a Shirley background subtraction and Gaussian (80%)–Lorentzian (20%) decomposition parameters. Atomic ratios were calculated from the peak areas that were calibrated by the sensitive factors provided by the equipment manufacturer.

NH_3-TPD spectra were recorded on a Micromeritica Auto Chem 2920. The sample (100 mg) was pretreated at 500 °C in an Ar flow of 20 ml min^{-1} for 1 h and then cooled down to 100 °C to be introduced with NH_3. The spectra were recorded from 100–700 °C with a rate of 5 °C min^{-1}. The quantities of weak, medium, and strong acid sites are measured by the amounts of ammonia desorbed at 100–200, 200–300, and 300–600 °C, respectively, through integrating the NH_3-TPD profile in each temperature interval. The apparatus and pretreated condition in the H_2-TPR experiment were the same as with NH_3-TPD. After cooling down to room temperature and introducing the reduction agent 10% H_2/Ar (30 ml min^{-1}), the sample was heated up to 900 °C from room temperature at a rate of 5 °C min^{-1}. The amount of H_2 uptake during the reduction was measured by a thermal conductivity detector (TCD), which was calibrated by the quantitative reduction of CuO to the metallic copper.[25]

Diffuse reflectance infrared spectra were measured by a Bruker Tensor 27 with a MCT detector (64 scans, 4 cm^{-1}). The catalyst was placed in an *in situ* IR cell equipped with KBr windows (Harrick). After heating at 400 °C for 2 h and evacuating at 10^{-4} bar, the cell was cooled down to the reaction temperature and the spectrum was recorded. Next, a gas mixture of DME and O_2 (nDME/$n$$O_2$ = 1 : 1) was introduced into the cell, and the spectra of catalyst adsorption were recorded. Finally, the catalyst desorption spectra were recorded after 30 min of reaction and the pressure of the cell was evacuated to 10^{-3} bar. Thermogravimetric/derivative thermogravimetry TG/DTG was measured on a NETZSCH STA 409 PC analyzer. The sample weight was about 10 mg. The temperature was ramped to 800 °C at a heating rate of 10 °C min^{-1} in an air flow of 50 ml min^{-1}.

2.3 Catalytic tests and analytic procedures

The catalytic test was performed in a continuous-flow fixed-bed reactor with an inner diameter of 10 mm. The catalyst (40–60 mesh) was diluted with SiO_2 (20–40 mesh). Before reaction, the catalyst was pretreated in an oxygen (99.999%) flow (25 ml min^{-1}) at 400 °C for 1 h. The reactant mixture consisted of DME and O_2 (nDME/$n$$O_2$ = 1 : 1), and the gas hourly space velocity (GHSV) was 800 h^{-1}. The outlet stream line from the reactor to the gas chromatograph was heated at 150 °C. The DME, toluene, MF, methanol, DMM, and formaldehyde products were analyzed by a gas chromatograph (GC-2060) equipped with a thermal conductivity detector (TCD) and a Porapak Q column (3 m × 3 mm), a gas chromatograph (Agilent 7890A) with flame ionization detectors

Table 1 Textural and structural properties of different catalysts

Catalyst	W content (wt.%) ICP	W content (wt.%) XPS	S_{BET} (m^2 g^{-1})	V_{micro} (cm^3 g^{-1})	V_{meso} (cm^3 g^{-1})
23.3 W/HZSM-5	23.3	25.4	216.35	0.086	0.054
34.9 W/HZSM-5	34.9	36.6	177.88	0.066	0.072
46.1 W/HZSM-5	46.1	46.2	121.73	0.048	0.034
51.1 W/HZSM-5	51.1	52.7	113.33	0.045	0.032
56.0 W/HZSM-5	56.0	56.9	111.56	0.042	0.022

(FIDs) (HP-PLOT capillary column), and a TCD (5 A molecular sieve) for analyzing alkanes, olefins, H_2, CO and CO_2.

3. Results and discussion

3.1 XRD and textural characterization

XRD patterns of HZSM-5 and W/HZSM-5 catalysts with different W contents are shown in Fig. 1. The parent HZSM-5 sample exhibits the characteristic peaks of an MFI structure (at 2θ of 7.9°, 8.9°, 23.07°, 23.6° and 24.4°) and quartz phase at 2θ of 26.6° (PDF number 89-1961).[26] However, with an increase in the W content, these diffraction lines of HZSM-5 decrease in intensity. Meanwhile, new lines characteristic of cubic WO_3 (at 2θ of 23.64°, 33.64°, 41.46° and 54.57°, PDF number 46-1096) and monoclinic WO_3 (at 2θ of 23.12°, 23.59°, 24.38°, 34.16° and 49.95°, PDF number 43-1035) are observed for the W/HZSM-5 catalysts. As for the 23.3 and 34.9 wt.% W/HZSM-5 catalysts, the split of the peaks at 23.1° and 23.6° are highly likely to be caused by their overlapping with the HZSM-5 zeolite characteristic bands at 23.07°, 23.64° and 24.4°. Moreover, the overlapping peaks become less obvious with the W content increasing from 46.1 to 56.0 wt.%, that is because the crystallinity of HZSM-5 zeolite decreases remarkably, pointing to a possible deterioration effect of tungsten species on the framework of HZSM-5 zeolite. Meanwhile, the intensities of the peaks at 23.6° and 24.4° increase obviously, which suggests that the fraction of the monoclinic phase of WO_3 increases with increasing W content.

The surface area data of the HZSM-5 and W/HZSM-5 catalysts with different W contents obtained by the N_2 adsorption method are shown in the Table 1. Obviously, the introduction of W species leads to a decrease of the surface area. With a W content from 23.3 to 56.0 wt.%, the surface area decreases from 216.35 to 111.56 $m^2\ g^{-1}$. The porous structure of W/HZSM-5 is also affected by introducing different W loadings. In general, the microporous volume of W/HZSM-5 zeolites is decreased by increasing W content. Although most of WO_3 particles are located on the surface, as revealed by the XPS results, they still may partially block the HZSM-5 microchannels and reduce the accessibility of micropores (Table 1). Moreover, the mesoporous volume of W/HZSM-5 increases first and then decreases with increasing W loading. These mesopores may be somewhat like inter-crystalline mesopores built among the stacked nano-crystals, which is related to an agglomerative morphology.[27] However, with the W content increasing to some further extent, the inter-crystalline voids may be reduced, and the mesoporous volume decreased.

However, the changes of the surface area and porous structure are more pronounced for the W/HZSM-5 with a low W content from 23.3 to 46.1 wt.% and the downward trends tend to flatten as the W content exceeds 46.1 wt.%. Furthermore, these changes are in agreement with the conversion of DME, which may be due to W domains partially covering the acid sites on the surface. Comparing the catalysts before and after the reaction, the BET surface area and micropore volume apparently decrease, which may be because the conversion of DME mainly occurs at the micropore channel of zeolite, and excessive carbon deposits cover the surface of the catalysts and in turn block the pores.

3.2 State of tungsten in HZSM-5

To determine the structure and coordination states of tungsten species with different contents, UV-vis DRS of W/HZSM-5 catalysts were recorded. As shown in Fig. 2, all the catalysts present three absorption bands at 230, 280 and 380 nm. The peak at 230 nm is associated with tetrahedrally monomeric tungstate species ($[WO_4]^{2-}$), and the bands located at 280 and 380 nm can be assigned to octahedral polytungstate species ($[WO_6]^{n-}$) and WO_3 crystallites respectively.[28] Therefore, three types of tungsten species exist in W/HZSM-5 catalysts. With increasing W content, the intensities of the three bands reinforce. When the content is 23.3 wt.%, the intensity of the band at 230 nm is stronger

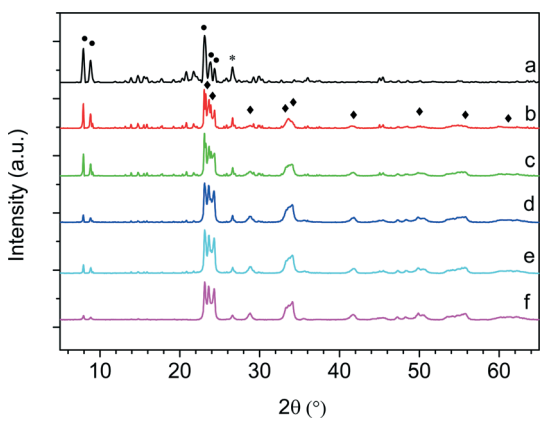

Fig. 1 The XRD patterns of catalysts: (a) HZSM-5, (b) 23.3 W/HZSM-5, (c) 34.9 W/HZSM-5, (d) 46.1 W/HZSM-5, (e) 51.1 W/HZSM-5, and (f) 56.0 W/HZSM-5. Crystalline phases detected: •, HZSM-5, ♦,WO_3.

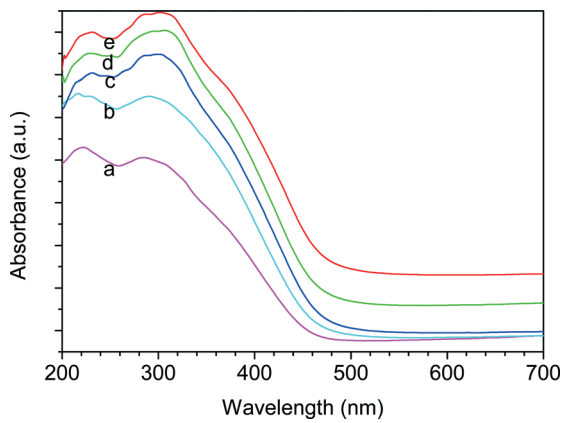

Fig. 2 UV-vis spectra of W/HZSM-5 catalysts with different W contents: (a) 23.3 wt.%, (b) 34.9 wt.%, (c) 46.1 wt.%, (d) 51.1 wt.%, and (e) 56.0 wt.%.

than that at 280 nm, and when the W content exceeds 34.9 wt.%, the peak at 280 nm becomes the dominant band. That is to say the tungsten species for the samples with low W content (23.3–34.9 wt.%) present mainly as $[WO_4]^{2-}$ tetrahedral species, and the tungsten domains for the samples with high content (34.9–56.1 wt.%) are primarily $[WO_6]^{n-}$ octahedral polytungstate species. These may be related to the change of the crystallite phase, as demonstrated by XRD.

The XPS survey spectra of W/HZSM-5 with different W contents were carried out. Fig. 3 presents XPS spectra of the W_{4f} region for W/HZSM-5 catalysts with different tungsten contents. The binding energies of W^{6+}, W^{5+} and W^{4+} are 37.3, 36.2 and 35.2 eV for $4f_{5/2}$ and 35.1, 33.6, and 32.9 eV for $4f_{7/2}$, respectively.[29,30] In the 23.3 wt.% W/HZSM-5 catalyst, W species with about 93.5% W^{6+} and 6.5% W^{5+} atoms were detected. With increasing W content, the amount of W^{6+} increases and of W^{5+} decreases, and when the W content reaches 56.0 wt.%, WO_3 becomes completely oxidized with 100% W^{6+}, as shown in Table 2. It was reported that the structure of monoclinic WO_3 tended to be completely oxidized,[29] and hence the change in chemical states is related to the change of WO_3 phase, as indicated by XRD.

The XPS spectra of O 1s shown in Fig. 4 show two BE peaks for all of the W/HZSM-5 catalysts with different tungsten contents. The lower BE band at about 530.3 eV corresponds to O^{2-} anions of tungsten oxide, and the higher BE band at 532.5 eV corresponds to O^{2-} anions associated with the HZSM-5 and surface hydroxides on the W/HZSM-5, both in physically adsorbed and chemically bonded forms.[29,31] With increasing W content, the amount of the O^{2-} anions of tungsten oxide increases to the maximum (38.04%) in 51.1 W/HZSM-5 and then decreases to 31.03% in the 56.0 W/HZSM-5. As for the O^{2-} species at 532.5 eV, the relative amount decreases from 82.72% in 23.3 W/HZSM-5 to 61.96% in 51.1 W/HZSM-5 and then increases to 68.96% in the 56.0 W/HZSM-5 catalyst. It is reasonable that the amount of O^{2-} anions associated with the HZSM-5 decreases, because the content of HZSM-5 decreases with the increasing W content, and the latter increase should be ascribed to the surface hydroxides on the W/HZSM-5, because the monoclinic WO_3 contains more surface OH groups and water molecules on the surface, compared with other WO_3 phases, as reported by Firkala.[29] This means that the surface OH species associated with tungsten oxide increases with increasing W content, which can influence the acidic properties of the W/HZSM-5 catalyst.

In summary, the results of UV-vis DRS and XPS demonstrate that the chemical state of W species changes with increasing W content. The tetrahedral $[WO_4]^{2-}$ species changes to $[WO_6]^{n-}$ octahedral polytungstate species, and W^{6+} is the main chemical state of tungsten in all the W/HZSM-5 catalysts. However, more surface OH species appear on W/HZSM-5 with a higher W content, which can influence the acidic properties of W/HZSM-5.

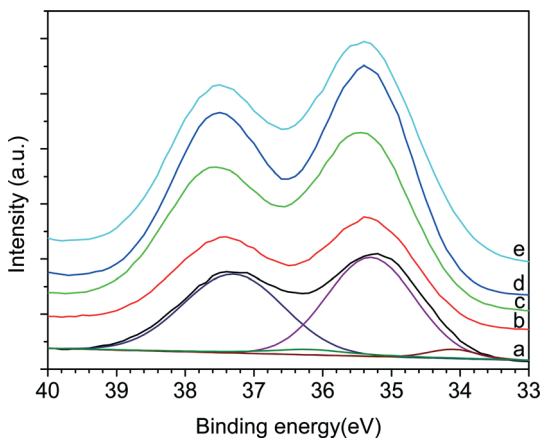

Fig. 3 XPS spectra of the W_{4f} region for different W/HZSM-5 catalysts: (a) 23.3 wt.%, (b) 34.9 wt.%, (c) 46.1 wt.%, (d) 51.1 wt.%, and (e) 56.0 wt.%.

3.3 Acidic properties

The concentration and strength of acid sites in W/HZSM-5 catalysts are determined by NH_3-TPD, as presented in Fig. 5. Generally, a NH_3-TPD profile of the HZSM-5 zeolite shows two desorption peaks, *i.e.* the high-temperature one located above 300 °C and the low-temperature one situated below 200 °C, which are ascribed to ammonia adsorbed on the strong and weak acid sites, respectively.[27] In this work, the distribution of the acid sites across the acidic strength is determined by integrating the NH_3-TPD profiles in different temperature intervals, as listed in Table 2, where the quantities of weak, medium, and strong acid sites are measured by the amounts of ammonia desorbed at 100–200, 200–300, and 300–600 °C, respectively. The W content exhibits a significant influence on the distribution of acid sites in W/HZSM-5. With the W content increasing, the total acid quantity decreases. It seems that the amount of the strong acid sites is increased with the W content increasing from 23.3 to 34.9 wt.%, and then decreased with the W content increasing to 56.0 wt.%. As for the amount of weak acid sites, it decreased with the W content increasing from 23.3 to 51.1 wt.%, and then it increases from 0.18 to 0.24 mmol g^{-1} with the W content increasing to 56.0 wt.%, as shown in Table 2. Undoubtedly, these are related to the cooperation between tungstate species and HZSM-5. As the XPS and UV-vis DRS results demonstrate, the octahedral polytungstate domains could accommodate a proton by electron transfer and charge delocalization across an extended W–O network and form some acidic sites.[32]

3.4 Redox properties

H_2-TPR profiles of W/HZSM-5 with different W contents are shown in Fig. 6, and the quantitative result is listed in Table 2. H_2-TPR has been extensively used to characterize the reducibility of oxygen species in WO_3- and WO_x-containing materials. It was found that bulk WO_3 can be reduced to W metal at temperatures below 927 °C. Three overlapping peaks

Table 2 NH_3-TPD, H_2-TPR and XPS results for the W/HZSM-5 catalysts

	Acid sites[a] (mmol g^{-1})				Redox sites[b] (mmol g^{-1})			Chemical state[c] (%)			
Catalysts	Weak	Medium	Strong	Total	Low	High	Total	W^{6+}	W^{5+}	O–W	O–HZSM-5
23.3 W/HZSM-5	0.64	0.63	0.86	2.13	0.55	3.20	3.75	93.5	6.5	17.28	82.72
34.9 W/HZSM-5	0.39	0.59	1.04	2.02	1.0	5.20	6.20	95.9	4.1	19.35	80.65
46.1 W/HZSM-5	0.27	0.43	0.83	1.53	1.44	6.58	8.02	97.6	2.4	32.46	67.54
51.1 W/HZSM-5	0.18	0.28	0.54	1.0	1.75	8.13	9.88	98.7	1.3	38.04	61.96
56.0 W/HZSM-5	0.24	0.27	0.48	0.99	1.77	8.48	10.25	100	0	31.03	68.96

[a] Density of the acid sites, assorted according to the acidic strength, determined by NH_3-TPD. [b] "Low" and "High" represent, respectively, the low temperature and high temperature band in H_2-TPR profiles shown in Fig. 5. The density of the redox sites is determined by H_2-TPR. [c] The change of the relative amounts of W and O species of different chemical states, "O–W" and "O–HZSM-5", represent the O^{2-} anions of tungsten oxide and the O^{2-} anions associated with the O–Si, O–Al and O–H on the W/HZSM-5.

were detected for the reduction of bulk WO_3 samples, which occurs *via* a stepwise reduction: $WO_3 \rightarrow WO_{2.9} \rightarrow WO_2 \rightarrow W$.[32] The reduction profiles for W/HZSM-5 samples have three overlapping peaks (Fig. 6) that occur at similar temperatures (about 550, 730 and 810 °C) with all W concentrations. These three peaks correspond to the same three reduction steps found in bulk WO_3 above. While the second peak at about 730 °C becomes obvious with increasing W concentration, it was reported that the second reduction step ($WO_{2.9} \rightarrow WO_2$) is sensitive to the dispersion of WO_x domains.[32] At a low W concentration (23.3 wt.%), there are not enough WO_x neighbors in these highly dispersed domains to form the stable intermediate WO_2 species, so a large fraction of the WO_x domains bypass this second reduction step and instead reduce directly to W metal ($WO_{2.9} \rightarrow W$) in the third reduction step. With the W content increasing from 34.9 to 56.0 wt.%, the WO_x surface densities become higher, the WO_x polyhedra are connected by W–O–W bonds, and there are enough WO_x neighbors to share the reduced charge and the H_2-TPR profiles exhibit an obvious reduction step from $WO_{2.9}$ to WO_2. Anyway, the amount of redox sites of the W/HZSM-5 catalysts is positive when correlated with the W content. The amount of redox sites increased from 3.75 to 10.25 mmol g^{-1} with the W content increasing 23.3 to 56.0 wt.%, as shown in Table 2.

3.5 Catalytic performance

The catalytic performances of W/HZSM-5 with different W contents in DME conversion under an O_2 stream are illustrated in Fig. 7. As for the conversion of DME, it decreases with increasing W content. When the W contents are 23.3 and 34.9 wt.%, the DME conversion is above 99.0%. As the W content reaches 46.1 wt.%, the DME conversion decreases to 82.6%, and then the conversion is almost unchanged; although the W content increases, DME conversion keeps at 80.8% and 87.0% for 51.1 and 56.0 wt.% W/HZSM-5, respectively. Obviously, the W content has an influence on the product distribution. The W/HZSM-5 catalysts with W content from 23.3 to 51.1 wt.% show high selectivity for toluene; however, when the W content becomes 56.0 wt.%, the toluene selectivity decreases to about 29.6%. When the W contents are 23.3 and 34.9 wt.%, there is nearly no methanol and CO, the main side-products are DMM, HCHO, MF and C_xH_y (CH_4, C_2H_4, C_3H_6, C_3H_8). With the W content increasing from 23.3 to 51.1 wt.%, the selectivity for CH_3OH increases first and then decreases, and the selectivity for HCHO

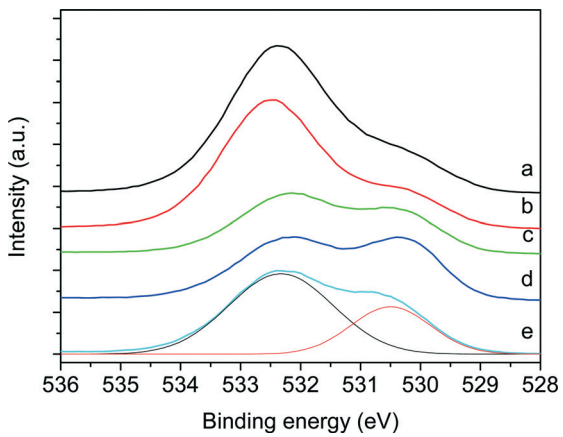

Fig. 4 XPS spectra of the O_{1s} region for different W/HZSM-5 catalysts: (a) 23.3 wt.%, (b) 34.9 wt.%, (c) 46.1 wt.%, (d) 51.1 wt.%, and (e) 56.0 wt.%.

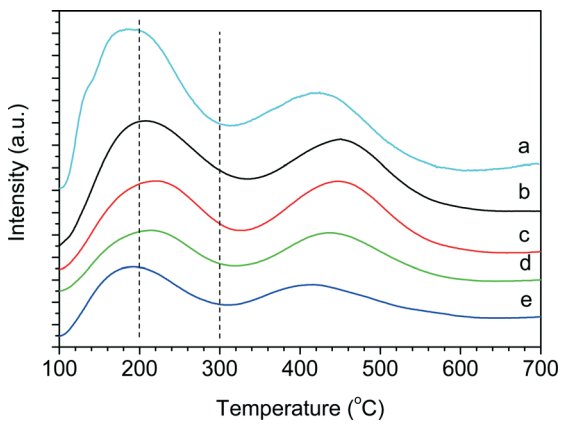

Fig. 5 NH_3-TPD spectra of W/HZSM-5 with different W contents: (a) 23.3 wt.%, (b) 34.9 wt.%, (c) 46.1 wt.%, (d) 51.1 wt.%, and (e) 56.0 wt.%.

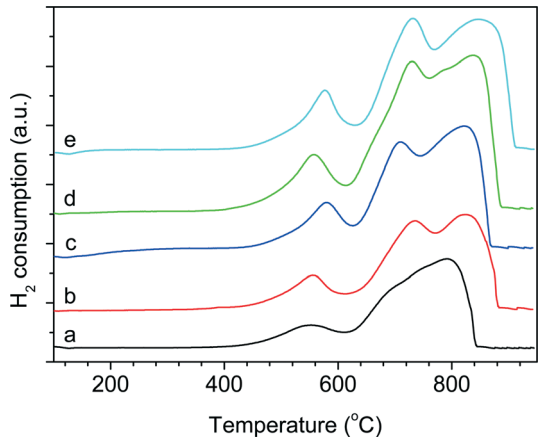

Fig. 6 H_2-TPR profiles of W/HZSM-5 catalysts with different W contents: (a) 23.3 wt.%, (b) 34.9 wt.%, (c) 46.1 wt.%, (d) 51.1 wt.%, and (e) 56.0 wt.%.

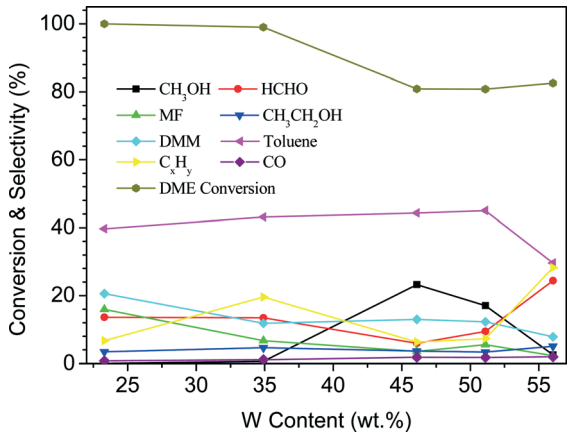

Fig. 7 Catalytic performance of DME conversion over W/HZSM-5 catalysts with different W contents.

decreases first and then increases, with the highest CH_3OH and HCHO selectivity at about 23.2% and 24.4%, which are achieved over the 46.1 wt.% and 56.0 wt.% W/HZSM-5 catalysts. Meanwhile, the selectivities for MF and DMM decrease with increasing W content. The 34.9 and 56.0 wt.% W/HZSM-5 catalysts have relatively high selectivity for C_xH_y. However, for all of the W/HZSM-5 catalysts with different W contents, no CO_2 is detected and only small amounts of CO and ethanol formed.

These catalytic results suggest that the W content not only influences the selectivity for toluene but also the selectivities for oxygen-containing chemicals such as HCHO, DMM and MF. It is understandable that the change in DME conversion has a similar tendency to the total amount of acid sites of W/HZSM-5 with different W contents, because the acid sites are the main active sites for DME activation. DME molecule could be easily activated to generate CH_3-, CH_3O-, and CH_3OCH_2-groups in the presence of O_2. Then these active groups can form toluene and C_xH_y through an acidic catalysis process, and meanwhile they can also form DMM, MF and HCHO over redox sites. However, with increasing W content, the number of redox sites increases to some extent, the DMM and MF may be oxidized further to CO, and hence the selectivities for MF and DMM slightly decrease and a small amount of CO is produced with the W content increasing to 56.0 wt.%. Meanwhile, with an increasing W content, the WO_3 chemical state changes. And when the W content exceeds 46.1 wt.%, monoclinic WO_3 becomes the dominant phase, which makes the nature of the acid sites change; this may be the main reason for the variation in the product state, especially for the change of CH_3OH selectivity. As indicated in Table 2, although the total acid sites decrease generally, the relative ratio of the amount of medium to strong acid sites is similar, 30%, 30%, 28%, 28% and 28% for 23.3, 34.9, 46.1, 51.1 and 56.0 wt.% W/HZSM-5, respectively. This may be the reason why the former four catalysts have similar toluene selectivity. Moreover, as for the 56.0 wt.% W/HZSM-5, acid site redistribution cannot be omitted. The ratio of the amount of weak acid sites increases and the amount of strong acid sites decreases, besides which the amount of redox sites increases to a maximum; this kind of chemical environment may favor the formation of HCHO and C_xH_y, therefore, the toluene selectivity decreases and the selectivities for HCHO and C_xH_y increase in the 56.0 W/HZSM-5 catalyst.

3.6 Catalytic mechanism of DME to toluene over W/HZSM-5

Fig. 8 depicts the IR spectra of DME/O_2 adsorption and desorption on the 46.1 wt.% W/HZSM-5 catalyst. After purification under vacuum conditions, infrared spectra of the catalysts show some bands in the OH stretching region at 3200–3800 cm^{-1}. These are associated with the framework aluminum [Si(OH)Al] (3610 cm^{-1}), the isolated external silanol groups (3745 cm^{-1}), free internal silanol groups (3728 cm^{-1}), and delocalized hydrogen-bonded groups (3500 cm^{-1}) of lattice defects, the partially hydrolyzed framework Al (around 3660 cm^{-1}) and the band of 3338 cm^{-1} can be ascribed to the OH stretching associated with W species,[33,34] As for the

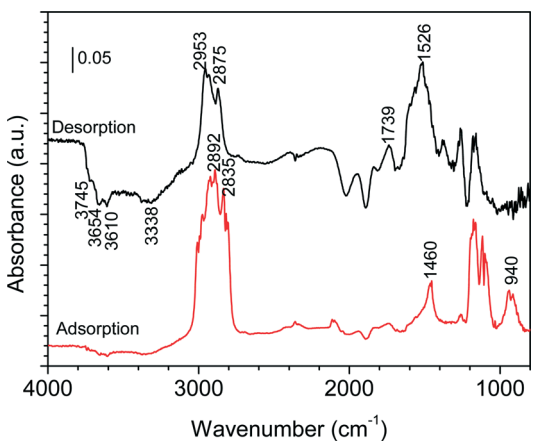

Fig. 8 DRIFTS spectra of DME/O_2 co-adsorption in (1% DME + 1% O_2)/Ar flow on the 46.1 wt.% W/HZSM-5 catalyst.

adsorption spectra, they show typical DME adsorption bands with a C–O–C stretching vibration at 1100–1200 cm^{-1}, a C–H stretching vibration at 2800–3000 cm^{-1} and a C–H deformation vibration at about 1400–1600 cm^{-1}. In addition, the bands that appear at 900–1000 cm^{-1} can be ascribed to the heterocyclic –C–O–C– asymmetric stretching.[35] However, in the desorption spectra, the bands at 900–1000 cm^{-1} disappear, which suggests that this kind of species should be attributed to the intermediate reactant formed through the adsorption of DME on the catalyst surface. Meanwhile, the bands of the O–H stretching region, which are related to the Brønsted acid groups in W/HZSM-5, reduce greatly, and strong multiple absorption bands at 2800–3100 cm^{-1} and 1400–1600 cm^{-1} are observed. These two bands are related to C–H and C–C stretching in the multisubstituted benzene.[35] The band at 1739 cm^{-1} can be ascribed to the C═O groups, which may be related to the formation of oxygen-containing chemicals such as HCHO, DMM and $HCOOCH_3$. These results may demonstrate that the formation of toluene over W/HZSM-5 catalyst may be accordance with the MTH reaction process on HZSM-5 with the acidic sites involved.

Meanwhile, the deactivated catalysts with different W contents were investigated by TG. Fig. 9 shows the profiles of the deactivated catalysts with 34.9, 46.1 and 51.1 wt.% W contents. There are two peaks of weight loss at 150 and 450 °C, which are attributed to coke formation on the external surface and inside the zeolite voids, respectively.[36] Obviously, the weight loss of the deactivation catalyst decreased with increasing W content. The BET results (Table 1) show that the fresh catalyst surface area decreases with increasing tungsten content, which indicates that the W content affects the external surface of the catalyst; the more the W content, the less the coke formation. This may be due to the introduction of tungsten covering the surface acid sites, as demonstrated by NH_3-TPD.

The characteristic pore structure of the HZSM-5 zeolite makes it the archetypical catalyst for the conversion of methanol/DME to hydrocarbon, and hence tremendous

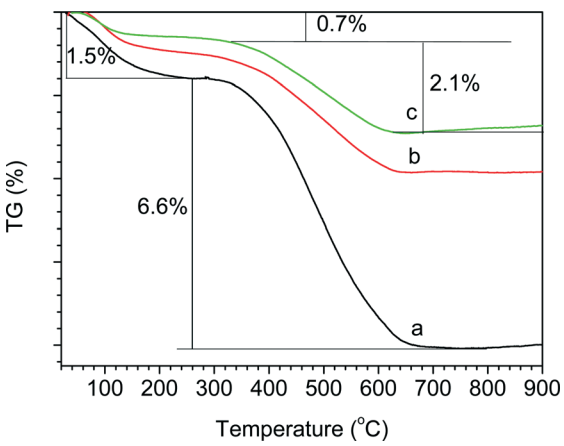

Fig. 9 TG profiles of W/HZSM-5 catalysts with different W contents: (a) 34.9 wt.%, (b) 46.1 wt.%, and (c) 51.1 wt.%.

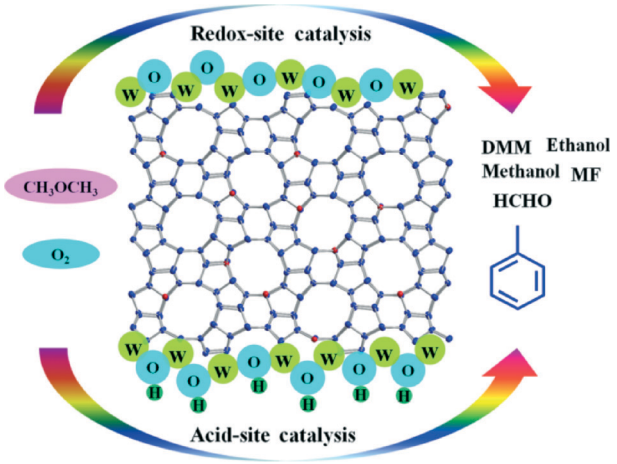

Fig. 10 Reaction pathway of DME over W/HZSM-5 catalysts in the presence of O_2.

efforts have been spent on elucidating the mechanism, varying from an autocatalytic mechanism to a hydrocarbon-pool mechanism. The dual-cycle concept, first introduced by Olsbye's group,[37] demonstrates the formation of ethylene and C_{3+} olefins more reasonably, being acknowledged as a refinement of the hydrocarbon-pool mechanism. It consists of the olefin-based methylation/interconversion cycle mainly producing C_{3+} alkenes and the aromatic-based cycle involving the formation of ethylene and aromatics. Though it is arguable whether the dual cycle operates independently or is mutually dependent, the fact that the aromatics are constantly formed in olefin-based cycle through the aromatization of higher alkenes, and also that ethylene is generated from the aromatic-based cycle, has been proved by numerous kinetic experimental data.[38] Therefore, it can be imagined that the target product could be obtained through facilitating or suppressing the operation of certain cycles by selecting a catalyst with a special topology and acidity.

Combined with the product distribution, a high selectivity for toluene was obtained and ethylene was the largest proportion among C_xH_y, and from the FT-IR results, the conversion of DME to toluene over W/HZSM-5 should obey the famous dual cycle of the MTH reaction on HZSM-5, and the aromatic-based cycle may be promoted by the synergistic effect of tungsten and ZSM-5 zeolites in the W/HZSM-5 catalyst. With the introduction of an amount of W that covers the surface acidic sites and partially breaks the cycle at toluene, the formation of higher methylbenzenes is effectively limited. Based on these results, a possible transformation pathway of DME conversion over W/HZSM-5 zeolite is deduced preliminarily, as shown in Fig. 10. For one side, the oxygenic groups might be converted to methanol, DMM, ethanol and MF over the redox sites of W/HZSM-5. For the other side, the groups might undergo an acid catalysis reaction to produce hydrocarbon-pool species under the cooperation of an acid site and a special pore channel, and toluene obtained.

4. Conclusions

A novel synthesis route for toluene from dimethyl ether has been efficiently performed over W/HZSM-5. The nature of the tungsten species, the distribution of acid sites, the redox properties, and the subsequent catalytic performance of W/HZSM-5 in DME conversion to toluene were influenced by the W content. Obviously, the introduction of W in HZSM-5 can bring about new redox sites which are relevant to the formation of the oxygen containing chemicals such as HCHO, DMM and MF and so on. With increasing W content, the octahedral polytungstate domains become the primary species, which favor the formation of new acidic sites associated with W, although the introduction of a high content of W can cover lots of acidic sites in HZSM-5. In this way, the existence of W prevents coke formation and may break the dual cycle of the DME-to-hydrocarbons reaction in HZSM-5 at toluene, and the formation of higher methylbenzenes is effectively limited. When the W content is up to 51.1 wt.%, the selectivity for toluene reaches 45% with the DME conversion decreasing from about 99% to about 80%, and with the W content increasing further, the selectivity for toluene decreases to about 29.3%. This may be related to the redistribution of the active acidic sites with a high content of W.

Acknowledgements

The authors are grateful for financial support by the Chinese Academy of Sciences Research Program (no. XDA07070301), the National Science Foundation of China (no. 21403264) and the National Science & Technology Pillar Program during the 12th Five-year Plan, China (No. 2010BAC66B03), the Qingdao Institute of Bioenergy and Bioprocess Technology Director Innovation Foundation for Young Scientists (Grant No. CASKLB201502) and the Applied Basic Research Programs of Qingdao (Grant Nos. 14-2-4-53-jch and 13-CX-19).

References

1 G. Yang, X. San, N. Jiang, Y. Tanaka, X. Li, Q. Jin, K. Tao, F. Meng and T. Noritatsu, *Catal. Today*, 2011, **164**, 425.
2 R. Khoshbinab and M. Haghighi, *Catal. Sci. Technol.*, 2014, **4**, 1779.
3 J. Sun, G. Yang, Y. Yoneyama and N. Tsubaki, *ACS Catal.*, 2014, **4**, 3346.
4 Z. Li, J. Li, M. Dai, Y. Liu, D. Han and J. Wu, *Fuel*, 2014, **121**, 173.
5 H. Zhou, Y. Wang, F. Wei, D. Wang and Z. Wang, *Appl. Catal., A*, 2008, **341**, 112.
6 Y. Li, M. Zhang, D. Wang, F. Wei and Y. Wang, *J. Catal.*, 2014, **311**, 281.
7 Q. Zhang, Y. Tan, C. Yang, H. Xie and Y. Han, *J. Ind. Eng. Chem.*, 2013, **19**, 975.
8 M. Boronat, C. Martinez and A. Corma, *Phys. Chem. Chem. Phys.*, 2011, **13**, 2603.
9 H. Liu, P. Cheung and E. Iglesia, *J. Catal.*, 2003, **217**, 222.
10 Q. Zhang, Y. Tan, C. Yang and Y. Han, *Catal. Commun.*, 2008, **9**, 1916.
11 Q. Zhang, Y. Tan, G. Liu, C. Yang and Y. Han, *J. Ind. Eng. Chem.*, 2014, **20**, 1869.
12 G. Liu, Q. Zhang, Y. Han, N. Tsubaki and Y. Tan, *Green Chem.*, 2013, **15**, 1501.
13 X. San, Y. Zhang, W. Shen and N. Tsubaki, *Energy Fuels*, 2009, **23**, 2843.
14 A. Corma, C. Martínez and E. Doskocil, *J. Catal.*, 2013, **300**, 183.
15 J. Li, C. Hu, K. Tong, H. Xiang, Z. Zhu and Z. Hu, *RSC Adv.*, 2014, **4**, 44377.
16 K. Barbera, S. Sørensen, S. Bordiga, J. Skibsted, H. Fordsmand, P. Beato and T. V. W. Janssens, *Catal. Sci. Technol.*, 2012, **2**, 1196.
17 J. Francisco, *Combust. Flame*, 1999, **117**, 312.
18 J. E. Herrera, J. H. Kwak, J. Hu, Y. Wang, C. H. F. Peden, J. Macht and E. Iglesia, *J. Catal.*, 2006, **239**, 200.
19 N. A. Saidina Amin and S. E. Pheng, *Catal. Commun.*, 2006, **7**, 403.
20 X. Yang, R. Gao, W. Dai and K. Fan, *J. Phys. Chem. C*, 2008, **112**, 3819.
21 R. Bi, X. Wang, Z. Liu and J. Chen, *J. Nat. Gas Chem.*, 2008, **17**, 332.
22 J. Yang, F. Deng, M. Zhang, Q. Luo and C. Ye, *J. Mol. Catal. A: Chem.*, 2003, **202**, 239.
23 G. Liu, Q. Zhang, Y. Han and Y. Tan, *Catal. Commun.*, 2012, **26**, 173.
24 B. Wang, H. Wang, G. B. Liu, Z. Li, X. M. Li and J. H. Wu, *J. Fuel Chem. Tech.*, 2014, **42**, 994.
25 H. Wang, H. Q. Zhu, Z. F. Qin, F. X. Liang, G. F. Wang and J. G. Wang, *J. Catal.*, 2009, **264**, 154.
26 M. Conte, B. Xu, T. E. Davies, J. K. Bartley, A. F. Carley, S. H. Taylor, K. Khalid and G. J. Hutchings, *Microporous Mesoporous Mater.*, 2012, **164**, 207.
27 X. Niu, J. Gao, Q. Miao, M. Dong, G. Wang, W. Fan, Z. Qin and J. Wang, *Microporous Mesoporous Mater.*, 2014, **197**, 252.
28 Q. Zhao, S. Chen, J. Gao and C. Xu, *Transition Met. Chem.*, 2009, **34**, 621.
29 T. Firkala, B. Fórizs, E. Drotár, A. Tompos, A. L. Tóth, K. Varga-Josepovits, K. László, M. Leskelä and I. M. Szilágyi, *Catal. Lett.*, 2014, **144**, 831.
30 B. Hu, H. Liu, K. Tao, C. Xiong and S. Zhou, *J. Phys. Chem. C*, 2013, **117**, 26385.
31 M. Occhiuzzi, D. Cordischi, D. Gazzoli, M. Valigi and P. C. Heydorn, *Appl. Catal., A*, 2004, **269**, 169.
32 D. G. Barton, S. L. Soled, G. D. Meitzner, G. A. Fuentes and E. Iglesia, *J. Catal.*, 1999, **181**, 57.
33 M. Bjøgen, S. Svelle, F. Joensen, J. Nerlov, S. Kolboe, F. Bonino, L. Palumbo, S. Bordiga and U. Olsbye, *J. Catal.*, 2007, **249**, 195.
34 J. Cao, B. Luo, H. Lin, B. Xu and S. Chen, *Appl. Catal., B*, 2012, **288**, 111.
35 *The Sadtler Handbook of Infrared Spectra, Informatics Division*, Bio-Rad Laboratories, Inc., 1978–2004, pp. 102 and 34.
36 A. Corma, C. Martínez and E. Doskocil, *J. Catal.*, 2013, **300**, 183.
37 S. Svelle, F. Joensen, J. Nerlov, U. Olsbye, K. P. Lillerud, S. Kolboe and M. Bjørgen, *J. Am. Chem. Soc.*, 2006, **128**, 14770.
38 U. Olsbye, S. Svelle, M. Bjørgen, P. Beato, T. V. W. Janssens, F. Joensen, S. Bordiga and K. P. Lierud, *Angew. Chem., Int. Ed.*, 2012, **51**, 5810.

